2019

Simultaneous Wick and Fluid Selection for the Design of Minimized-Thermal-Resistance Vapor Chambers under Different Operating Conditions

K. Baraya
Purdue University

J. A. Weibel
Purdue University, jaweibel@purdue.edu

S V. Garimella
Purdue University, sureshg@purdue.edu

Baraya, K.; Weibel, J. A.; and Garimella, S V., "Simultaneous Wick and Fluid Selection for the Design of Minimized-Thermal-Resistance Vapor Chambers under Different Operating Conditions" (2019). *CTRC Research Publications.* Paper 341.
http://dx.doi.org/https://doi.org/10.1016/j.ijheatmasstransfer.2019.03.025

Simultaneous wick and fluid selection for the design of minimized-thermal-resistance vapor chambers under different operating conditions

Kalind Baraya, Justin A. Weibel[1], Suresh V. Garimella
School of Mechanical Engineering
Purdue University, 585 Purdue Mall, West Lafayette, IN 47907 USA

Abstract

The thermal resistance of a vapor chamber is primarily governed by conduction across the evaporator wick and the saturation temperature gradient in the vapor core. The relative contributions of these two predominant resistances can vary dramatically with vapor chamber operating conditions and geometry. In the limit of very thin form factors, the contribution from the vapor core thermal resistance dominates the overall thermal resistance of the vapor chamber; recent work has focused on working fluid selection to minimize overall thermal resistance in this limit. However, the wick thermal resistance becomes increasingly significant as its thickness increases to support higher heat inputs while avoiding the capillary limit. It therefore becomes critical to simultaneously consider the contributions of the wick and vapor core thermal resistances in the development of a generalized methodology for vapor chamber working fluid selection. The current work uses a simplified thermal-resistance-network-based vapor chamber model to explore selection of working fluids and wick structures that offer the minimum overall thermal resistance as a function of the vapor chamber thickness and heat input. An illustrative example of working fluid selection, for cases with and without the contribution of wick thermal resistance, is first used to demonstrate the potential significance of the wick thermal resistance on fluid choice. This influence of the wick on working fluid selection is further explained based on the wick properties (effective pore radius, permeability, and effective thermal conductivity). The ratio of effective pore radius to wick permeability is found to be the most critical wick parameter governing the overall vapor chamber resistance at thin form factors where minimizing the wick thickness is paramount; the wick conductivity becomes an equally important parameter only at thicker form factors. Based on this insight, a new approach for vapor chamber design is demonstrated, which allows simultaneous selection of the working fluid and wick that provides minimum overall thermal resistance for a given geometry and operating condition.

[1] Corresponding author, E-mail address: jaweibel@purdue.edu.

Keywords: Vapor chamber, heat pipe, wick, working fluid, thermal resistance

Nomenclature

a_1,	constants in R_{wick} relation [-]	U_r	maximum radial velocity (m/s)
a_2, b_1	constants in R_{vap} relation [-]	z	axial coordinate (m)
D	particle diameter (m)		
F_s	factor of safety	***Greek symbols***	
h_{fg}	latent heat of vaporization (J/kg)	ρ	density (kg/m^3)
K	wick permeability (m^2)	σ	surface tension (N/m)
k	thermal conductivity (W/m K)	μ	dynamic viscosity (N s/m^2)
$\dot{m}$	mass flow rate (kg/s)	φ	porosity
M_l	liquid figure of merit (W/m^2)		
M_v	vapor figure of merit (W/m^3 K)	***Subscript***	
$\dot{m}_{wick,c}$	mass flow rate in condenser wick (kg/s)	cu	copper
$\dot{m}_{wick,e}$	mass flow rate in evaporator wick (kg/s)	l	liquid
P	pressure (N/m^2)	v	vapor
P_{cap}	capillary pressure (N/m^2)	vap	vapor core
Q	heat load (W)	wick	wick
r	radial coordinate (m)		
R	thermal resistance (W/K)		
r_c	condenser radius (m)		
Re	Reynolds number $\left(\rho UR/\mu\right)$ (-)		
r_e	evaporator/heater radius (m)		
r_{eff}	effective pore radius (m)		
R_g	gas constant (J/kg K)		
R_{total}	total thermal resistance (W/K)		
T	temperature (K)		
t	working thickness (m)		
t_{vap}	vapor core thickness (m)		
t_{wick}	wick thickness (m)		
u_r	radial velocity (m/s)		

1. Introduction

Heat pipes and vapor chambers are extensively employed in the thermal management of electronics. A vapor chamber is a passive phase-change-based device that effectively transports or spreads heat, leading to a relatively small thermal resistance. Figure 1 schematically depicts the operation of a vapor chamber. A wick structure lining the inside of the vapor chamber provides the capillary pressure that passively drives the fluid flow loop. The evaporator is continuously fed with fluid that evaporates and absorbs latent heat. The vapor thus formed condenses and releases this heat at the condenser region, which thus acts as a heat sink [1]. Given their passive operation and reliability, vapor chambers have been used as heat spreaders in a multitude of applications ranging from low to high heat fluxes and thin to thick form factors [2–5]. Proper selection of the wick and fluid pair suitable for particular form factors and heat loads is critically important to the design of vapor chambers.

Owing to the widespread use of vapor chambers for electronics cooling, their design has been studied extensively over the last two decades using both analytical and numerical modeling techniques. Vafai and Wang [6] developed a steady-state analytical model to predict vapor flow, pressure distribution, and temperature fields in asymmetric flat heat pipes. The model assumes negligible vapor flow in the axial direction, and thus the velocity and pressure profiles were obtained in the lateral plane. The analytical expressions obtained were compared against the solution of flow-field equations for conventional symmetric flat heat pipes, and good agreement was observed. Prasher [7] modeled vapor chambers as an effective conduction-based thermal resistance network to predict the steady-state temperature characteristics. Based on the model, they defined two performance parameters, namely the heat transport capacity (heat transfer rate at a fixed temperature drop) and heat carrying capacity (capillary-limited heat transfer rate). These performance parameters were used as the basis for selection of the wick thickness. Vadakkan *et al.* [8] developed a numerical model for analyzing the transient thermal performance of vapor chambers, and explored the effect of vapor core thickness on vapor pressure drop; higher heat loads could be applied to thicker vapor cores due to a reduction in the vapor core pressure drop. Ranjan *et al.* [9] used this numerical modeling approach to optimize the thermal performance of 1 mm-thick vapor chambers. It was concluded that vapor core resistance becomes significant at low vapor core thicknesses and decreases with increase in heat load and vapor core thickness. Moreover, a decrease in wick thickness leads to a lower wick thermal resistance but higher pressure drop in the wick. Based on these observations, wick thicknesses

were proposed to optimize the thermal and hydrodynamic performance of the vapor chamber across low and high heat loads, respectively.

Fluid selection plays an important role in the performance of a vapor chamber. A common metric for fluid selection is based on a figure of merit that considers all the *liquid* properties affecting the capillary limit of the vapor chamber M_l [1]:

$$M_l = \frac{\rho_l \sigma h_{fg}}{\mu_l}. \tag{1}$$

The value of M_l determines the maximum heat carrying capacity of a vapor chamber based on the capillary pressure head available to overcome the viscous flow resistance in the wick, also known as the capillary limit; the higher the value of M_l, the higher is the capillary limit of the vapor chamber for a given wick structure. As reflected in the expression for M_l, a fluid with higher latent heat of vaporization and higher liquid density would transport more heat per unit volume, while a lower liquid viscosity would lead to lower pressure drop in the wick, and a higher surface tension would increase the capillary pressure. Fluid selection based on M_l is suitable for vapor chambers having thick form factors where pressure drop in the vapor core is negligible, and when the performance objective is to maximize the heat load.

Yadavalli *et al.* [10] used a thermal resistance network model to assess the effective thermal resistance of vapor chambers at thin form factors. The effective thermal resistance of the vapor chamber in this case is dominated by the high pressure drop (and thereby high saturation temperature difference) in the vapor core. Hence, the fluid selection for vapor chambers with thin form factors, when the performance objective is minimizing the vapor core thermal resistance, was recommended to be based on the *vapor* figure of merit, M_v, given as

$$M_v = \frac{P_v h_{fg}^2 \rho_v}{R_g T_v^2 \mu_v}, \tag{2}$$

which contains the vapor properties affecting the thermal resistance of the vapor core. A higher value of M_v yields a lower vapor core thermal resistance at a given thickness.

While these figures of merit can guide fluid selection based on singular performance objectives of either maximizing heat load or minimizing vapor core resistance, a more nuanced vapor chamber performance objective is required in practice: achieving a minimum thermal resistance while avoiding the capillary limit at a target operating power. A vapor chamber design approach, in this case, cannot simply consider a single figure of merit such as M_l or M_v for fluid selection. Patankar *et al.* [11] developed a coupled fluid selection and wick thickness design approach to achieve optimized thermal performance for thin vapor chambers. In

this approach, the vapor chamber was designed to have the minimum wick thickness required to sustain the imposed heat load without suffering a capillary limit, so as to maximize the space made available to the vapor core and thus minimizing the vapor pressure drop and thermal resistance. It was shown that working fluid selection using this design approach should be based on a combination of both M_l and M_v in addition to the given heat load. However, this approach [11] is valid only for thin form factors at which the vapor core thermal resistance dominates, and does not consider the impact of the wick thermal resistance or wick properties that become critical at thick form factors and high heat loads.

A critical element of vapor chamber design is the wick, which performs the primary function of transporting the condensed fluid back to the evaporator via capillary action to sustain closed-loop, passive operation. The wick must provide a high capillary pressure while also having large permeability to minimize the pressure drop through the wick. Several different types of wicking structures have been incorporated into vapor chambers (e.g., grooves, screen meshes, sintered powders, micropillar arrays, etc.); however, usually a single type of wick cannot serve the needs of all applications, as different types of wicks present trade-offs between heat transport capability and minimized thermal resistance. There have been several novel wick designs aimed at either increasing maximum heat flux [2] or reducing wick thermal resistance [12–16], or even achieving desired temperature profiles on the condenser side [17]. However, the implications of wick properties on choosing a wick for minimization of the total thermal resistance of the vapor chamber have not been systematically explored in the literature. Furthermore, there has been no attempt to develop a holistic approach for working fluid selection in concert with the choice of wick, despite the interrelationship of their functionality.

In the current work, we assess the effects of governing wick properties on vapor chamber design, in terms of fluid and wick selection at various operating conditions. Using a resistance-network-based modeling approach, a closed-form analytical expression for vapor chamber thermal resistance is developed that accounts for all relevant wick and working fluid properties. The model is then used to study the influence of various wick properties on the thermal performance of a vapor chamber with respect to operating conditions, based on which a method for simultaneous fluid and wick selection is proposed and demonstrated.

2. Model

The geometry of the vapor chamber is shown in Figure 1. For modeling purposes, the vapor chamber can be divided into three separate zones: wall, wick, and vapor core. The wall is the solid region that encloses the wick and vapor core regions. A heat load is directly applied to the evaporator region of the wall on one

face of the vapor chamber. The opposite side of the vapor chamber responsible for heat rejection is referred to as the condenser region. The wick adjacent to the evaporator region is referred to as the evaporator-side wick, whereas the wick on the opposing side is the condenser-side wick.

To model the thermal transport in the vapor chamber, a one-dimensional thermal resistance network is considered with each component of the vapor chamber being modeled as an effective thermal resistance. This simplified modeling approach has proven effective in various studies [7,10,18,19] that have sought to explore the design space at low computational cost.

As the thermal resistance posed by conduction through the wall of the vapor chamber remains independent of the internal design, the current study considers only the contributions to thermal resistance from the wick and vapor core regions. The disc-shaped vapor chamber considered here has a circular heater input region of radius of r_e at the center of the evaporator face. The wick and vapor core regions have the same radial dimensions, equal to the entire condenser-side face, with radius denoted by r_c. The condenser and evaporator wicks are assumed to have equal thickness t_{wick} and the vapor core thickness is t_{vap}; the total working thickness is defined as $t = 2t_{wick} + t_{vap}$ since the wall is not included in the analysis.

The following subsections detail the model development and assumptions. The model represents the total thermal resistance of the vapor chamber, including both the wick (Section 2.1) and vapor core (Section 2.2) resistances, in the form of a closed analytical expression containing the thermophysical properties of the fluid, physical properties of the wick, and geometric parameters of the vapor chamber. The model can then be used to assess the influence of wick properties on wick and fluid selection at different operating conditions (namely, heat load Q and working thickness t).

2.1. Wick thickness and thermal resistance

In the vapor chamber wick, it is assumed that a one-dimensional, incompressible radial flow exists with pressure drop and velocity varying according to Darcy's law for fluid flow in porous media. As a result, body and inertial forces are neglected and the pressure gradient is equated to the viscous resistance. The radial pressure gradient in the wick is given by

$$\frac{dP_{wick}}{dr} = -\frac{\mu_l}{K} u_{r,l}(r), \tag{3}$$

where fluid velocity in the wick is related to mass flow rate as

$$u_{r,l}(r) = \frac{\dot{m}_{\text{wick}}(r)}{\rho_l 2\pi r t_{\text{wick}}}. \tag{4}$$

In the evaporator-side wick, uniform evaporation is assumed to occur from the wick into the vapor core over the heat input area. Outside the heat input area ($r > r_e$), it is assumed that no evaporation occurs and the mass flow at each radial cross section is constant. Thus, on the evaporator side, a piecewise expression for mass flow rate in the evaporator wick is given as

$$\begin{aligned} \dot{m}_{\text{wick,e}}(r) &= -\frac{Q}{h_{fg}} \text{ for } r > r_e \\ \dot{m}_{\text{wick,e}}(r) &= -\frac{Q}{h_{fg}}\left(\frac{r}{r_e}\right)^2 \text{ for } 0 < r < r_e \end{aligned}. \tag{5}$$

The vapor is assumed to condense uniformly over the condenser side, and hence mass flow rate in the condenser-side wick can be expressed as

$$\dot{m}_{\text{wick,c}}(r) = \frac{Q}{h_{fg}}\left(\frac{r}{r_c}\right)^2 . \tag{6}$$

To find the total pressure drop, equation (3) is integrated over both the evaporator and condenser wick, with limits of integration from $r = 0$ to $r = r_c$, and using the expressions of mass flux in equations (5) and (6). This yields an expression for the total pressure drop in the wick as

$$\Delta P_{\text{wick}} = \frac{\mu_l Q}{2\pi h_{fg} \rho_l t_{\text{wick}} K}\left\{\ln\left(\frac{r_c}{r_e}\right) + 1\right\}. \tag{7}$$

A key characteristic of the wick is the capillary pressure available to drive the fluid flow. The capillary pressure depends on the surface tension of the fluid and effective pore radius of the wick material, and is given as

$$P_{\text{cap}} = \frac{2\sigma}{r_{\text{eff}}}. \tag{8}$$

Equation (8) describes the maximum capillary pressure that can be sustained by the wick; if the total pressure drop in the wick exceeds this capillary pressure, then the evaporator wick will not be replenished with working fluid, and will dry out (i.e., the capillary limit). The premise of the current design approach is to minimize the thermal resistance of the vapor chamber while operating within the capillary limit. This can be achieved by designing for the minimum wick thickness that utilizes the complete capillary pressure head available [11]; at this minimum thickness, both the wick and vapor core thermal resistances will be

minimized. Introducing a factor of safety, and equating equations (7) and (8), the expression for wick thickness is obtained, as

$$t_{\text{wick}} = \frac{QF_s r_{\text{eff}}}{4\pi M_l K}\left\{\ln\left(\frac{r_{\text{c}}}{r_{\text{e}}}\right)+1\right\}, \tag{9}$$

where M_l is the liquid figure of merit defined in equation (1). For the present study, F_s is taken as unity.

To compute the total thermal resistance of the evaporator and condenser wick, uniform, one-dimensional axial heat conduction is assumed in the two wick regions. The total thermal resistance can be expressed as

$$R_{\text{wick}} = \frac{t_{\text{wick}}}{k_{\text{wick}}\pi r_{\text{e}}^{\,2}} + \frac{t_{\text{wick}}}{k_{\text{wick}}\pi r_{\text{c}}^{\,2}} = a_1 Q\left(\frac{1}{k_{\text{wick}}}\frac{r_{\text{eff}}}{K}\right)\left(\frac{1}{M_l}\right) \tag{10}$$

$$\text{where} \quad a_1 = \frac{F_s}{4\pi^2}\left\{\ln\left(\frac{r_{\text{c}}}{r_{\text{e}}}\right)+1\right\}\left(\frac{1}{r_{\text{e}}^2}+\frac{1}{r_{\text{c}}^2}\right)$$

2.2. Vapor core thermal resistance

The vapor core thermal resistance is associated with the pressure gradient (and hence the saturation temperature gradient) due to the vapor flow. It is assumed based on a scaling arguments that $\text{Re}\times(t_{\text{vap}}/r_{\text{e}})^2$ is small (where Re is the Reynolds number, expressed as $\frac{\rho_v U_{r,v} r_{\text{c}}}{\mu_v}$), and thus axial momentum transport is predominantly diffusion-governed and the contribution of convective terms is negligible (in the axial direction). Thus, the conservation of linear momentum equation in cylindrical coordinates is simplified to obtain

$$\frac{dP_{\text{vap}}}{dr} = \mu_v \frac{d^2 u_{r,\text{vap}}(r,z)}{dz^2{}_{\text{vap}}}. \tag{11}$$

Equation (11) is integrated across the vapor core thickness to obtain the radial velocity in terms of the radial pressure drop, assuming no-slip boundary conditions on both walls of the vapor core, that is $u_r(r,-t_{\text{vap}}/2)=0$ and $u_r(r,t_{\text{vap}}/2)=0$. Thus, the vapor velocity in the axial direction is

$$u_{r,v}(r,z) = -\frac{t^2{}_{\text{vap}}}{8\mu_v}\frac{dP_{\text{vap}}}{dr}\left(1-\frac{4z^2{}_{\text{vap}}}{t^2{}_{\text{vap}}}\right). \tag{12}$$

Given the prior assumption that fluid evaporates from evaporator-side wick uniformly over the heat input area, and that condensation occurs uniformly over the condenser-side wick surface, the mass flow rate through the vapor core as a function of the heat input is given as

$$\begin{aligned} \dot{m}_{\text{vap}}(r) &= \frac{Q}{h_{fg}}\left(\frac{r^2}{r_{\text{e}}^2}-\frac{r^2}{r_{\text{c}}^2}\right) \text{ for } r< r_{\text{e}} \\ \dot{m}_{\text{vap}}(r) &= \frac{Q}{h_{fg}}\left(1-\frac{r^2}{r_{\text{c}}^2}\right) \text{for } r> r_{\text{e}} \end{aligned}. \tag{13}$$

Moreover, at a given radial position, mass flow rate through the cross section is given as

$$\dot{m}_{\text{vap}}(r) = \int_{-t_{\text{vap}}/2}^{t_{\text{vap}}/2} 2\pi r\rho_v u_{r,v}(r,z)dz\,. \tag{14}$$

Thus, performing the integration shown in equation (14) utilizing the expression for vapor velocity from equation (12) yields

$$\dot{m}_{\text{vap}}(r) = -\frac{\pi\rho_v r t^3_{\text{vap}}}{6\mu_v}\frac{dP_v}{dr}\,. \tag{15}$$

To calculate the total pressure drop in the vapor core, equation (15) is integrated in the radial direction from the limit $r = 0$ to $r = r_{\text{c}}$, and using the mass flux from equation (13), to obtain

$$\triangle P_{\text{vap}} = \frac{6\mu_v Q}{\pi h_{fg}\rho_v t^3_{\text{vap}}}\ln\left(\frac{r_{\text{c}}}{r_{\text{e}}}\right). \tag{16}$$

This pressure drop can be related to temperature drop in the vapor core based on the Clausius-Clapeyron relation [20] as

$$\triangle T_{\text{vap}} = \frac{6R_g T_v^2\mu_v Q}{P_v\pi h_{fg}^2\rho_v t^3_{\text{vap}}}\ln\left(\frac{r_{\text{c}}}{r_{\text{e}}}\right). \tag{17}$$

Because $t_{\text{vap}} = t - 2t_{\text{wick}}$ where t_{wick} is specified by equation (9), the thermal resistance of the vapor core can be given as

$$R_{\text{vap}} = \frac{6}{\pi M_v (t - 2t_{\text{wick}})^3} \ln\left(\frac{r_c}{r_e}\right) = \frac{a_2}{M_v \left(t - b_1 Q \frac{1}{M_l} \frac{r_{\text{eff}}}{K}\right)^3} \quad (18)$$

where $a_2 = \frac{6}{\pi} \ln\left(\frac{r_c}{r_e}\right)$; $b_1 = \frac{F_s}{2\pi}\left\{\ln\left(\frac{r_c}{r_e}\right) + 1\right\}$

2.3. Total thermal resistance and model implementation

The total resistance of the vapor chamber is the summation of the effective resistances of the wick and vapor core in series:

$$R_{\text{total}} = R_{\text{wick}} + R_{\text{vap}} = a_1 Q \left(\frac{1}{k_{\text{wick}}} \frac{r_{\text{eff}}}{K}\right)\left(\frac{1}{M_l}\right) + \frac{a_2}{M_v \left(t - b_1 Q \frac{1}{M_l} \frac{r_{\text{eff}}}{K}\right)^3}, \quad (19)$$

in which the constants a_1, a_2, and b_1 are defined in equations (10) and (18), and the wick thickness is specified according to the design constraint given by equation (9).

This thermal resistance network model was implemented in the commercial software MATLAB [21]. The temperature-dependent thermophysical fluid properties were computed from the commercial database REFPROP [22].

3. Results and Discussion

3.1 Effect of wick resistance on working fluid selection

The expressions for wick and vapor core thermal resistance in equations (10) and (18), respectively, constitute the total thermal resistance imposed by the vapor chamber. From equation (19), it can be observed that besides its dependence on various wick, geometric, and operational parameters, the total thermal resistance is also a function of fluid properties, combined into liquid (M_l) and vapor (M_v) figures of merit. Hence, for a given operating condition (working thickness t and heat load Q), a working fluid can be selected from a given set of fluids that would provide the minimum thermal resistance. The fluid choice can thus be mapped on a t-Q map, where each point on the map represents the working fluid with properties that minimizes the total thermal resistance [11].

The vapor chamber considered for the current study has a heat input area of radius r_e = 5 mm and a condenser surface of radius r_c = 45 mm. The operating temperature of the vapor chamber is taken as T_v = 325 K, and all the thermophysical fluid properties are evaluated at this temperature. The wick considered for the analysis in this section has permeability of $K = 2.63 \times 10^{-10}$ m^2, porosity $\varphi = 0.5$, effective pore radius $r_{eff} = 1.42 \times 10^{-4}$ m, and thermal conductivity k_{wick} = 17.9 W/m-K.

Consider a set of three working fluids: pentane, acetone, and water. The fluids represent an extreme range of the liquid and vapor figures of merit that govern vapor chamber thermal resistance; it can be observed from Table 1 that among the three fluids, pentane has the highest M_v and water has the highest M_l, while acetone falls in the middle. This broad range of M_l and M_v values are used in this example to generalize the effects of these figures of merit on fluid selection.

Figure 2 maps the working fluids that would provide minimum resistance for a range of *t*-*Q* operating conditions. For instance, focusing on Figure 2 (a), if a vapor chamber is operating at a heat load of 6 W and has an available working thickness of 60 µm, it can be seen from the *t*-*Q* map that water would provide the minimum thermal resistance. On the other hand, for the same working thickness, if the operating heat load is reduced to 2 W, acetone would be the preferred working fluid based on the same map.

The fluid selection maps in Figure 2 are used as a case study to depict the influence of wick resistance over a range of working thicknesses using maps that neglect or consider wick resistance. Figure 2 (a) shows the fluid selection for a range of working thicknesses from 50 µm to 100 µm (thin form factors) when wick resistance is neglected, whereas Figure 2 (c) shows the fluid selection for same range of working thicknesses but with wick resistance included. In both cases (Figure 2 (a) and (c)), the optimal working fluid at a given *t*-*Q* operating condition does not change. At these thin form factors, the choice of fluid favors high M_v (e.g., pentane for the present case) at low input power, and transitions toward a higher M_l (e.g., water) with increasing working thickness and higher heat inputs.

These trends in the fluid property preferences can be explained based on the relative contributions of the wick and vapor core resistances at different operating conditions. At thin form factors, the vapor core resistance dominates the overall resistance of the vapor chamber, due to the high pressure drop in the vapor core. Under these conditions, a higher M_v value is beneficial as it directly reduces the vapor core pressure drop; however, a higher M_l value also provides an indirect benefit because the same heat load can be supported using a thinner wick, thereby making a greater portion of the working thickness available to the vapor core. Analyzing the expression for the vapor core resistance in equation (18), at a given working thickness, M_v becomes prioritized in the extreme of low heat loads (for which the working thickness is primarily occupied by the vapor core) and M_l is prioritized in the extreme of high heat loads (for which a

majority of the working thickness must be allotted to the wick). This tradeoff leads to the specific trends observed in Figure 2 (a) and (c), where the preferred fluid changes to that with a higher M_l as the heat load increases for a given working thickness. A detailed discussion of the mechanisms governing fluid choice based on the vapor core resistance alone is available in Ref. [11].

While the working fluid selection is not affected by the wick resistance at thin form factors, a dramatic influence at thicker form factors is revealed by comparing the *t*-*Q* maps shown in Figure 2 (b) and (d) for working thicknesses ranging from 50 μm to 500 μm. Only vapor core resistance is considered in Figure 2 (b), whereas both wick and vapor core resistance are considered in Figure 2 (d). The two figures differ remarkably in terms of the optimum working fluid for a given operating condition. In Figure 2 (b), the choice of working fluid follows the same trend and reasoning as discussed for Figure 2 (a) and (c) at all working thicknesses: a fluid with high M_v (pentane) is preferred at low heat load while one with a high M_l (water) is indicated at high heat loads. However, when wick resistance is considered in Figure 2 (d), the choice of fluid begins to strongly favor a high M_l as the working thickness increases, such that at a sufficiently large thickness, the fluid with high M_v (pentane) is never preferred.

The marked change in the choice of the optimal working fluid at thicker form factors with the wick resistance accounted for can be explained based on the fact that the conduction resistance across the wick becomes increasingly dominant relative to the vapor core resistance. As per equation (9), a higher M_l reduces the required wick thickness, thus lowering the wick thermal resistance. At a given heat load, for large working thicknesses, the relative importance of the vapor core resistance greatly diminishes; thus, fluid selection for M_l can be prioritized to minimize the wick thickness, regardless of the M_v value. Among the fluids considered, water has the highest M_l value, and therefore is preferred as a working fluid over a wide range of the operating heat load (Q) at high working thicknesses.

3.2 Importance of wick parameters in deciding overall vapor chamber thermal resistance

The working fluid selection case study in Section 3.1 showed that the wick thermal resistance has a prominent role at thick form factors, and must be taken into account while designing vapor chambers for minimized thermal resistance. It is thus important to explore the effects of wick parameters on the wick and vapor core thermal resistances, to inform selection of wicks that minimize the thermal resistance.

From equation (9), it is observed that the required wick thickness is linearly proportional to the ratio of effective pore radius to wick permeability (r_{eff} / K). Thus, an increase in effective pore radius or a decrease in wick permeability indirectly leads to an increase in wick thermal resistance, as given by equation (10); the wick thermal resistance (k_{wick}) also increases with a decrease in wick thermal conductivity. Moreover,

any change in r_{eff} / K affecting the required wick thickness has a concomitant change in the vapor core thickness, and hence vapor core thermal resistance. Thus, the wick parameters r_{eff} / K and k_{wick} impact the thermal resistance of the vapor chamber and therefore serve as figures of merit for the wick, akin to the fluid and vapor figures of merit that govern the thermal resistance of the vapor chamber. To assess the operating conditions (*t*-*Q*) for which these wick parameters play a governing role, a sensitivity analysis is performed. The sensitivity of the total vapor chamber resistance to the wick parameters r_{eff} / K and k_{wick} is evaluated as a function of operating conditions and form factor on a *t*-*Q* map. The sensitivity analysis is performed using the same vapor chamber physical geometry, baseline wick properties, and operating temperature as considered in the case study for fluid selection (Section 3.1). The working fluid for the present case study is water, with thermophysical properties evaluated at the operating temperature of the vapor chamber (325 K). We define the normalized sensitivity of the total vapor chamber thermal resistance to the parameters r_{eff} / K and k_{wick} as

$$\text{Sensitivity to } r_{\text{eff}} / K\text{: } \frac{\triangle R_{\text{total}}}{\triangle (r_{\text{eff}} / K)} \frac{(r_{\text{eff}} / K)}{R_{\text{total}}}\text{, and} \tag{20}$$

$$\text{Sensitivity to } k_{\text{wick}} = \frac{\triangle R_{\text{total}}}{\triangle k_{\text{wick}}} \frac{k_{\text{wick}}}{R_{\text{total}}}\text{,} \tag{21}$$

where R_{total} is computed at a given *t*-*Q* operating condition. The normalized sensitivity values obtained for r_{eff} / K and k_{wick}, for operating conditions in the range of working thickness (t) from 50-500 μm and heat load (Q) from 0.5-12 W, are plotted as contours on a *t*-*Q* map in Figure 3; a higher sensitivity value indicates that the corresponding wick property has more influence on overall thermal resistance of the vapor chamber in that region of the *t*-*Q* map. For example, for Q = 8 W at two different working thicknesses of t = 200 μm and t = 450 μm, Figure 3(a) shows that the thermal resistance has a normalized sensitivity value of 20 with respect to k_{wick} at t = 200 μm, versus 40 at t = 450 μm. This implies that thermal resistance is more sensitive to wick conductivity at the thicker form factor. Moreover, contour values at a given operating condition can be compared across Figure 3(a) and (b), due to the normalization. For example, at t = 450 μm and Q = 8 W, the higher normalized sensitivity to r_{eff} / K, a value of 60, implies that r_{eff} / K is a relatively more significant wick parameter than k_{wick} at this operating condition.

From Figure 3(a), the normalized sensitivity value for k_{wick} is seen to increase with increasing working thickness or heat load. Figure 3(b) shows that the sensitivity to r_{eff} / K always increases as heat load increases for a given working thickness. However, the variation of sensitivity to r_{eff} / K is a non-monotonic

function of the working thickness at a given heat load; the sensitivity value initially decreases (at small thicknesses) and then increases (at larger thicknesses) as the working thickness increases.

The sensitivity trends observed in Figure 3(a) and (b) can be explained in terms of how the wick properties affect the wick and vapor core resistances. From the working fluid selection discussed in Section 3.1, the wick resistance was found dominant in determining overall thermal resistance of a vapor chamber at thicker form factors and higher heat loads. Hence, as k_{wick} only affects the wick resistance (equation (10)), the sensitivity value for wick resistance monotonically increases as working thickness or heat load increase (Figure 3(a)). This same trend is observed for r_{eff} / K in Figure 3(b), but only at thicker form factors and higher heat loads where the wick resistance dominates; because r_{eff} / K also indirectly affects the vapor core resistance, the trend differs at thin form factors where the vapor core resistance is dominant. From equation (18), the vapor core resistance varies as the wick thickness-cubed (for a constant working thickness), and because wick thickness increases linearly with r_{eff} / K (equation (9)), the total resistance becomes very sensitive to r_{eff} / K at thin form factors. As working thickness increases for a given heat load, the relative contributions of the decreasing vapor core resistance and increasing wick resistance, both of which are influenced by r_{eff} / K, leads to a non-monotonic sensitivity of the total vapor chamber thermal resistance, as observed in Figure 3(b).

Moreover, on comparing the relative magnitudes of the sensitivities to k_{wick} and r_{eff} / K in Figure 3(a) and (b), k_{wick} and r_{eff} / K are seen to be equally important in determining the overall thermal resistance ($\frac{r_{eff}}{K} * \frac{1}{k_{wick}}$ governs the performance) at larger thicknesses, whereas the wick conductivity is not an important criterion (r_{eff} / K governs the performance) at smaller thicknesses. A strategy for wick selection across various operating conditions, based on the individual wick parameters, is discussed in the next section.

3.3 Wick selection for minimized thermal resistance at various operating conditions

The relative contribution of the wick resistance to the total vapor chamber thermal resistance as well as the sensitivity of the total resistance to various wick parameters have been discussed to this point as a function of operating conditions. The wick parameters are found to not only affect the wick resistance, but also have a significant, indirect effect on the vapor core resistance, and thereby influence the total vapor chamber thermal resistance across all operating conditions.

This section demonstrates a wick selection procedure for minimized vapor chamber thermal resistance over a range of operating conditions. As a case study, three example sintered copper powder wicks are chosen with different porosities (0.65-0.75) and particle diameters (of 2.0×10^{-5} m to 4.8×10^{-5} m), as given in Table 2. The permeability and effective pore radius are computed using the following correlations [20]

$$K = \frac{D^2\varphi^3}{150(1-\varphi)^2} \text{ , and,} \tag{22}$$

$$r_{\text{eff}} = 0.21D\,. \tag{23}$$

The wick conductivity is computed using the Maxwell-Eucken model [23]

$$k_{\text{wick}} = k_{\text{cu}}\frac{2k_{\text{cu}} + k_l - 2(k_{\text{cu}} - k_l)\varphi}{2k_{\text{cu}} + k_l + (k_{\text{cu}} - k_l)\varphi}\,. \tag{24}$$

Table 2 lists the calculated values for r_{eff} / K and $\frac{r_{\text{eff}}}{K} * \frac{1}{k_{\text{wick}}}$ for the three wick structures, which are the parameter groupings that affect the vapor core thermal resistance and wick thermal resistance, respectively. The geometric parameters and operating temperature (325 K) of the vapor chamber are identical to those specified in the working fluid selection study (Section 3.1).

Figure 4 shows the wick selection on a map of working thickness and heat load with *t* ranging from 50-500 μm and *Q* from 0.5-12 W. Note that the working fluid is fixed to be acetone. At a particular *t*-*Q* operating condition, Figure 4 maps the wick which provides the lowest overall thermal resistance for the vapor chamber; for example, at t = 400 μm and Q = 2 W, Wick 1 provides the minimum resistance.

It is observed from Figure 4 that Wick 3 emerges as the best choice at thin form factors, even though Wick 1 provides the lowest wick thermal resistance. The trend can be explained based on the conclusions drawn regarding the sensitivity analysis in Section 3.2. At thin form factors, r_{eff} / K determines the wick selection due to its influence on vapor core resistance; hence, Wick 3 would provide the minimum total resistance for the vapor chamber in the range of lower working thicknesses because it has the lowest r_{eff} / K of the three available wicks (Table 2). At thick form factors, the wick resistance is significant and depends on $\frac{r_{\text{eff}}}{K} * \frac{1}{k_{\text{wick}}}$. Hence, Wick 1 minimizes the overall thermal resistance. Wick 2 appears in the intermediate region, and is selected in a transitional region between thinner and thicker form factors. At high heat loads and small working thickness, the solid region in the lower right of Figure 4 signifies where none of the three wicks would be able to provide the required capillary pressure head.

3.4 Simultaneous wick and working fluid selection

The discussion to this point has demonstrated the method for selection of the working fluid (Section 3.1) and the wick (Section 3.3) based on minimizing overall thermal resistance as independent, decoupled case studies. However, the total vapor chamber resistance is inherently coupled to both the wick and fluid; selection of the wick and fluid cannot be made independently, but must consider the coupling of all properties at the desired operating condition for the vapor chamber.

To demonstrate simultaneous wick and working fluid selection, three working fluids (acetone, water, and pentane; properties shown in Table 1) and three wicks (shown in Table 2) are considered. The geometric parameters of the vapor chamber are identical to those specified in Section 3.1 (r_e = 5 mm, r_c = 45 mm) and the operating temperature is 325 K. For a given *t*-*Q* operating condition, the model is used to identify the combination of working fluid and wick that provides the lowest vapor chamber thermal resistance, which is then mapped across a range of working thicknesses (t = 50-500 μm) and heat loads (Q = 0.5-12 W). Figure 5 shows the *t*-*Q* map of these identified combinations of working fluid and wick.

The results in Figure 5 appear as a 'phase diagram', divided into various operating regions for which each wick and working fluid pair is preferred. The figure reveals the inter-dependent nature of wick and fluid selection, as depicted by sharp transition lines between the possible choices; while the reasons for these transitions can be attributed to the dependence of wick and vapor core resistances on wick and fluid properties as discussed in the previous sections, in sum, the specific shape of each region is a non-intuitive outcome requiring solution of the model. In Figure 5 we present a relatively simple decision matrix containing only three working fluids and wicks over a limited window of operation at a single temperature. However, this general methodology for simultaneous fluid-wick selection can be trivially extended to consider the myriad of possible candidate wicks and fluids, as well as operating ranges and temperature. The generalized methodology equips engineers with an ability to choose the best fluid-wick combination, out of all the possible combinations that arise in practical applications, for which this decision cannot be made based on intuition or any singular fluid/wick figure of merit.

4. Conclusions

A thermal-resistance-network-based, one-dimensional model was used to study and characterize the importance of the wick properties in governing the net thermal performance of a vapor chamber at different operating conditions (namely, working thicknesses and heat loads). The study first explored the relative significance of the wick thermal resistance on the overall vapor chamber thermal resistance, followed by

an analysis of the sensitivity of the overall vapor chamber thermal resistance to the wick properties. A methodology was then developed to enable the choice of a working fluid and wick combination that minimizes the overall resistance of the vapor chamber. This simultaneous wick and working fluid selection methodology mapped the ideal wick-fluid combination as a function of working thickness and heat load that is presented in the form of a phase diagram. The key conclusions of the study are:

1. Wick thermal resistance plays a significant role in determining the overall thermal resistance of the vapor chamber, compared to the vapor core thermal resistance, at relatively thick form factors and high heat loads.
2. At larger working thicknesses, the wick parameter grouping $\frac{r_{\text{eff}}}{K} * \frac{1}{k_{\text{wick}}}$ determines the wick thermal resistance, and thereby significantly affects the thermal resistance of the vapor chamber with increasing heat loads.
3. At small working thicknesses with increasing heat loads, the wick conductivity is not a crucial factor while making the wick selection. Rather, wick selection should be based only on r_{eff} / K, which affects the vapor core thermal resistance.
4. To obtain the best thermal performance in a vapor chamber, the working fluid and wick should be selected simultaneously; the total thermal resistance is highly coupled to both the working fluid and wick properties, and the best combination across different operation conditions cannot be mapped to any single parameter grouping.

References

[1] S.W. Chi, Heat pipe theory and practice: a sourcebook, (1976).

[2] J.A. Weibel, S. V. Garimella, Recent Advances in Vapor Chamber Transport Characterization for High-Heat-Flux Applications, Adv. Heat Transf. 45 (2013) 209–301.

[3] T. Shioga, Y. Mizuno, Micro loop heat pipe for mobile electronics applications, Annu. IEEE Semicond. Therm. Meas. Manag. Symp. (2015) 50–55.

[4] A. Faghri, Review and Advances in Heat Pipe Science and Technology, J. Heat Transfer. 134 (2012) 123001.

[5] H. Tang, Y. Tang, Z. Wan, J. Li, W. Yuan, L. Lu, Y. Li, K. Tang, Review of applications and developments of ultra-thin micro heat pipes for electronic cooling, Appl. Energy. 223 (2018) 383–400.

[6] K. Vafai, W. Wang, Analysis of flow and heat transfer characteristics of an asymmetrical flat plate heat pipe, Int. J. Heat Mass Transf. 35 (1992) 2087–2099.

[7] R.S. Prasher, A Simplified Conduction Based Modeling Scheme for Design Sensitivity Study of Thermal Solution Utilizing Heat Pipe and Vapor Chamber Technology, J. Electron. Packag. 125 (2003) 378.

[8] U. Vadakkan, J.Y. Murthy, S. V. Garimella, Transient Analysis of Flat Heat Pipes, Heat Transf. Vol. 3. (2003) 507–517.

[9] R. Ranjan, J.Y. Murthy, S. V. Garimella, D.H. Altman, M.T. North, Modeling and design optimization of ultrathin vapor chambers for high heat flux applications, IEEE Trans. Components, Packag. Manuf. Technol. 2 (2012) 1465–1479.

[10] Y. Yadavalli, J.A. Weibel, S. V Garimella, Performance-Governing Transport Mechanisms for Heat Pipes at Ultra-thin Form Factors, IEEE Trans. Components, Packag. Manuf. Technol. 5 (2015) 1618–1627.

[11] G. Patankar, J.A. Weibel, S. V. Garimella, Working-fluid selection for minimized thermal resistance in ultra-thin vapor chambers, Int. J. Heat Mass Transf. 106 (2017) 648–654.

[12] Q. Cai, Y.-C. Chen, Investigations of Biporous Wick Structure Dryout, J. Heat Transfer. 134 (2012) 021503.

[13] J.A. Weibel, S. V. Garimella, Visualization of vapor formation regimes during capillary-fed boiling in sintered-powder heat pipe wicks, Int. J. Heat Mass Transf. 55 (2012) 3498–3510.

[14] T. Semenic, I. Catton, Experimental study of biporous wicks for high heat flux applications, Int. J. Heat Mass Transf. 52 (2009) 5113–5121.

[15] R. Ranjan, S. V. Garimella, J.Y. Murthy, K. Yazawa, Assessment of nanostructured capillary wicks for passive two-phase heat transport, Nanoscale Microscale Thermophys. Eng. 15 (2011) 179–194.

[16] J.A. Weibel, S. V. Garimella, J.Y. Murthy, D.H. Altman, Design of integrated nanostructured wicks for high-performance vapor chambers, IEEE Trans. Components, Packag. Manuf. Technol. 1 (2011) 859–867.

[17] G. Patankar, J.A. Weibel, S. V. Garimella, Patterning the condenser-side wick in ultra-thin vapor chamber heat spreaders to improve skin temperature uniformity of mobile devices, Int. J. Heat

Mass Transf. 101 (2016) 927–936.

[18] M.T. Ababneh, F.M. Gerner, P. Chamarthy, P. de Bock, S. Chauhan, T. Deng, Thermal-Fluid Modeling For High Thermal Conductivity Heat Pipe Thermal Ground Planes, J. Thermophys. Heat Transf. 28 (2014) 270–278.

[19] I. Sauciuc, G. Chrysler, R. Mahajan, R. Prasher, Spreading in the heat sink base: Phase change systems or solid metals??, IEEE Trans. Components Packag. Technol. 25 (2002) 621–628.

[20] D.A. Reay, P.A. Kew, R.J. McGlen, Heat Pipes, 2014.

[21] MATLAB, Natick, Mathworks Inc, Massachusetts, United States. (2012).

[22] E.W. Lemmon, M.L. Huber, M.O. Mclinden, REFPROP 9.1, NIST Stand. Ref. Database. (2013).

[23] J.K. Carson, S.J. Lovatt, D.J. Tanner, A.C. Cleland, Thermal conductivity bounds for isotropic, porous materials, Int. J. Heat Mass Transf. 48 (2005) 2150–2158.

List of tables

List of figures

Table 1. Liquid and vapor figures of merit for the working fluids considered in this study (T = 325 K).

Fluid	M_l (W/m^2)	M_v (W/m^3 K)
Water	3.00×10^{11}	1.29×10^{13}
Acetone	3.06×10^{10}	2.32×10^{14}
Pentane	1.47×10^{10}	7.56×10^{14}

Table 2. Sintered powder wick porosity, particle diameter, and properties determining wick selection at various operating conditions.

Wick #	φ	D (m)	r_{eff}/K (m^{-1})	r_{eff}/K*1/k_{wick} (K/W)
1	0.65	4.80×10^{-5}	2.33×10^{5}	3.21×10^{3}
2	0.70	3.30×10^{-5}	2.50×10^{5}	2.82×10^{3}
3	0.75	2.00×10^{-5}	2.93×10^{5}	2.77×10^{3}

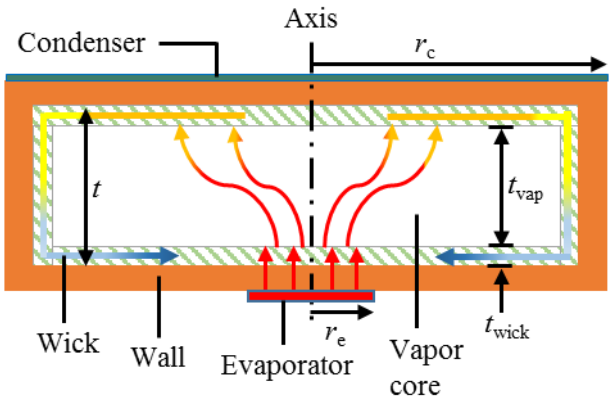

Figure 1: Schematic diagram of a vapor chamber.

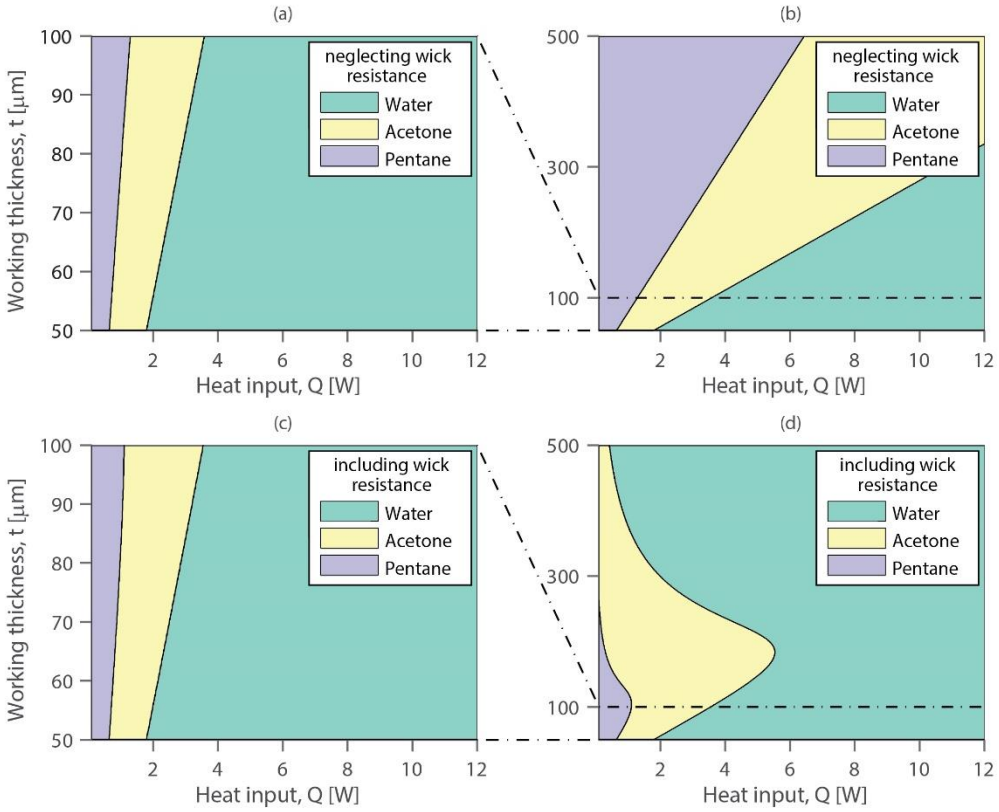

Figure 2. Working fluid selection maps for a vapor chamber as a function of working thickness *t* and heat input *Q* for minimized thermal resistance (i.e., *t*-*Q* map): at thin form factors (a) neglecting resistance of the wick and (c) considering wick resistance; and at thick form factors (b) neglecting resistance of the wick and (d) considering wick resistance. The region below the dashed line in (b) and (d) indicates the range of working thickness shown in (a) and (c), respectively. The fluid properties are given in Table 1.

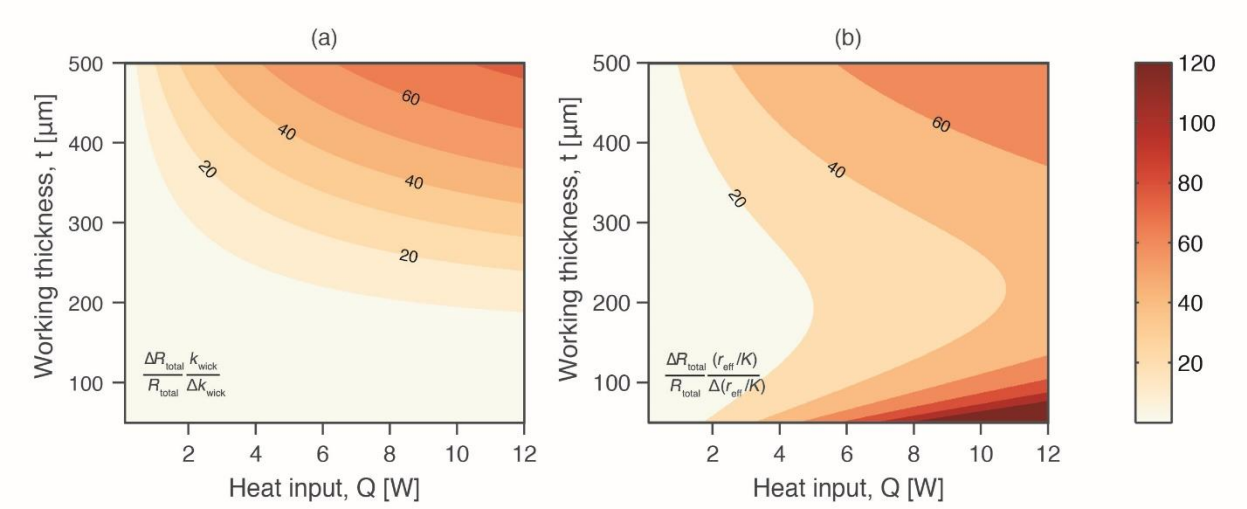

Figure 3. Contour plot of the normalized sensitivity of the total vapor chamber thermal resistance to the (a) wick conductivity (k_{wick}), and (b) ratio of effective pore radius to wick permeability (r_{eff}/K), as shown as a function of working thickness t and heat input Q (i.e., a t-Q map).

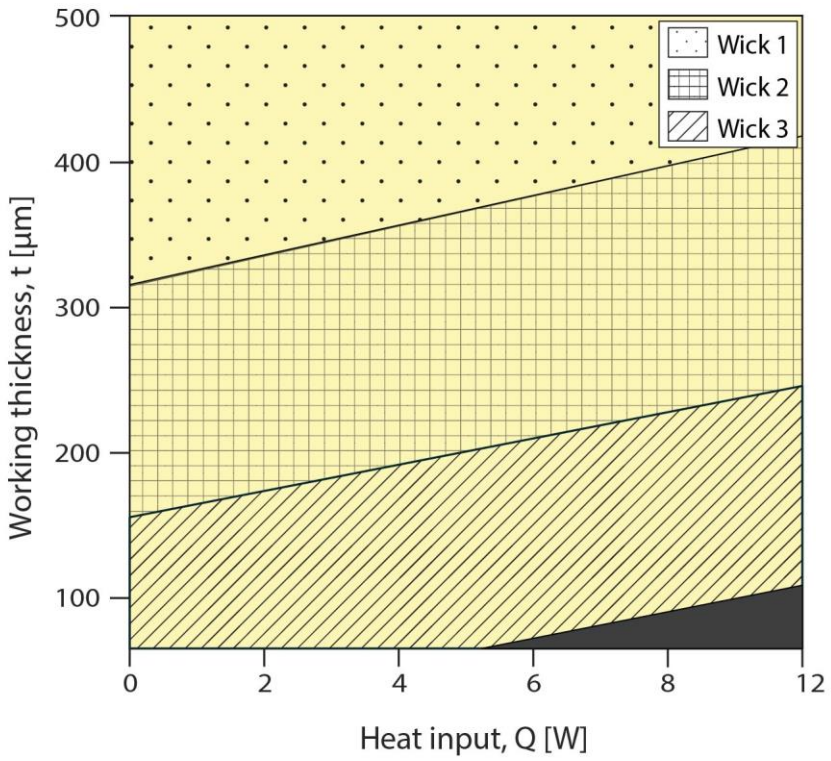

Figure 4. Wick selection map for a vapor chamber as a function of working thickness *t* and heat input *Q* for minimized thermal resistance (i.e., *t*-*Q* map) with acetone as a working fluid. The wick properties are given in Table 2.

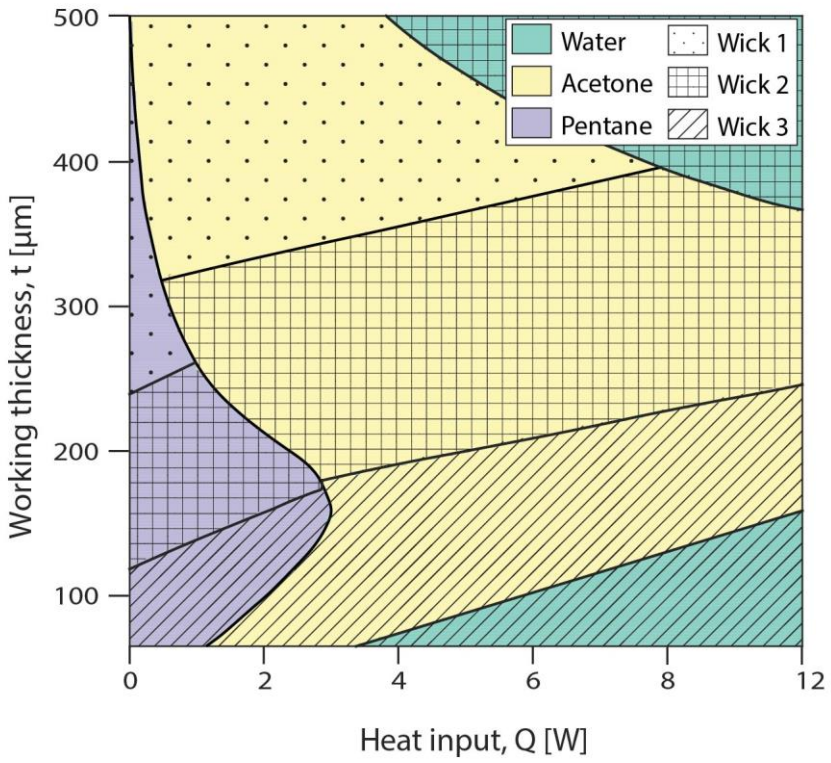

Figure 5. Simultaneous working fluid and wick selection map for a vapor chamber as a function of working thickness *t* and heat input *Q* for minimized thermal resistance (i.e., *t*-*Q* map). The fluid and wick properties are given in Table 1 and Table 2, respectively.